Journal of Molecular Liquids 289 (2019) 111135

Contents lists available at ScienceDirect

Journal of Molecular Liquids

journal homepage: www.elsevier.com/locate/molliq

On the interplay between the local structure and dynamics in low concentration mixtures of H_2O and HOD in the [$Emim^+$][TF_2N^-] room temperature ionic liquid

Ioannis Skarmoutsos *, Leonidas Spyrogiannopoulos, Emmanouil Kainourgiakis, Jannis Samios *

Department of Chemistry, Laboratory of Physical Chemistry, National & Kapodistrian University of Athens, Panepistimiopolis 157-71, Athens, Greece

ARTICLE INFO

Article history:
Received 20 February 2019
Received in revised form 2 June 2019
Accepted 4 June 2019

Keywords:
Ionic liquids
Water
Preferential solvation
Molecular dynamics
Rotational dynamics
Isotopic effects

ABSTRACT

Molecular Dynamics simulations have been employed to investigate the local structural and dynamic properties of low-concentrated water and HOD dissolved in an ionic liquid consisting of the 1-ethyl-3-methylimidazolium cation and the bis(trifluoromethylsulfonyl)imide anion. The results obtained disclose that the water molecules interpenetrate the ionic structural networks and interact with the anions and the cations of the ionic liquid. The calculations have also revealed a strong interaction between the oxygen atoms of the anion and the hydrogen atoms of the water molecules and a quite important interaction between the hydrogen atoms of the imidazolium ring with the water oxygen atoms. The translational and rotational diffusion of water molecules is almost one order of magnitude lower in comparison with pure water, but still one order of magnitude higher in comparison with the ionic liquid's anions and cations. The translational diffusion of the anions is lower than the diffusion of the cations, whereas the rotational diffusion is very similar. However, the reorientational dynamics of the anion and the cation is very anisotropic and the mechanisms of the rotation around different intramolecular axes take place at different time scales. The calculated orientational anisotropy of the O-D vector of HOD in the ionic liquid has been found to be in very good agreement with available experimental data, showing more pronounced differences with the O-H vector reorientational dynamics at long-time scales.

1. Introduction

Over the last two decades, ionic liquids (ILs) have received considerable attention due to their unique physical and chemical properties, which make them attractive sustainable solvents with enormous applicability across many areas of chemical science and engineering. A wide range of ILs can be generally synthesized by combining different organic cations and inorganic or organic anions. The ability to tune their properties by combining the appropriate anion-cation pairs is highly substantial, since it provides the opportunity to rationally design solvents for targeted chemical processes [1–11]. This fact has led to generally characterize ILs as "*designer solvents and additives*" [12]. Interestingly, many of these ILs are hygroscopic and the complete removal of water from them is nearly impossible [13–15]. While the existence of water impurities is known to alter the physical properties and chemical reaction rates in hygroscopic ILs [16–18], the presence of water as a cosolvent can usually reduce the viscosity of the IL solvent [19]. A deeper understanding of the modification of IL properties upon the addition of water can therefore provide valuable information with significant practical implications.

The investigation of water at dilute and low concentrations in an ionic liquid can also provide a deeper insight towards a better understanding of water-ion interactions. Up to now, as mentioned in previous studies, dilute aqueous salt solutions were used as a probe to study the nature of water-ion interactions. In these dilute solutions the ions are fully hydrated and water—water interactions are perturbed but still prevalent. On the other hand, the solutions of dilute or low concentrated water dissolved in an IL provide a unique opportunity to investigate these interactions. These systems resemble an ionic sea with isolated water islands, where the water—water interactions are negated and the behavior of the isolated water molecules can serve as a direct probe of the water-ion interactions [13].

According to previous studies reported in the literature, structural and energetic heterogeneities manifest in ILs in the form of frictionally stiff (charge and density enhanced) and frictionally soft (charge and density depleted) local environments [20–22]. When hydrogen bonding (HB) tracer solutes are small compared to the typical volume of cations and anions in an ionic liquid, their translational and rotational dynamic behavior reflects the local structural heterogeneities in the ILs and particularly the preferential solvation of the tracer solutes in specific nano-domains of the IL. The tracer diffusion through these

* Corresponding authors.
E-mail addresses: iskarmoutsos@hotmail.com (I. Skarmoutsos), isamios@chem.uoa.gr (J. Samios).

https://doi.org/10.1016/j.molliq.2019.111135
0167-7322/

distinct local environments and the IL reorientational dynamics may be also linked with significant deviations from Stokes-Einstein behavior [20–24].

Previous studies on hydrogen bonding in pure ILs have showed that preferential HB interactions and HB directionality play an important role in stabilizing the local structural networks within the liquids and have a strong impact on the transport and dynamic properties of the ILs [25–31]. It has also been found that the effect of the co-solvent addition, and in particular water, upon the IL properties depends strongly upon the HB network they form in the mixed solutions [32–40]. One of our main motivations in this present study was therefore to find out how the different water-anion and water-cation HB interactions affect not only the dynamics of the tracer water molecules, but also the dynamics of the anions and the cations. Particular attention has been paid on the investigation of the pair atomic residence dynamics between the water and specific HB binding sites of the anions and the cations and how the mechanisms of these relaxation processes can be related to the dynamics of the different rotational modes of the ions and the rotational dynamics of the O-H vector of the water molecules.

Interestingly, the dynamics of a series of small HB tracer molecules (water, methanol and ethanol) diluted to low concentration in the room temperature IL 1-ethyl-3-methylimidazolium bis (trifluoromethylsulfonyl)imide ([Emim$^+$][TF$_2$N$^-$]), was recently investigated by Fayer and coworkers [41] using 2D infrared vibrational echo (2D IR) spectroscopy and polarization resolved pump-probe experiments on the deuterated hydroxyl (O–D) stretching mode of each of the solutes. From these experiments the orientational correlation functions for these systems were obtained by measuring the orientational anisotropy, which can be directly related to the second-order Legendre reorientational time correlation function (tcf) [41–43]. This was an additional motivation for us to use [Emim$^+$][TF$_2$N$^-$] as the reference IL in our studies and directly compare our findings with these previously reported experimental data. Moreover, the isotopic effects on the mechanisms of the reorientational dynamics of water in [Emim$^+$][TF$_2$N$^-$] were further analyzed by investigating the reorientational dynamics of the O-D and O-H vectors of HOD and H_2O in the IL.

The paper is organized as follows: computational details are presented in Section 2, while our data and a comprehensive discussion of the results are presented in Section 3. The main conclusions and final remarks are summarized in Section 4.

2. Computational details

In the present study NPT and NVT MD simulation runs were performed for a binary mixture of [Emim$^+$][TF$_2$N$^-$] with water at constant temperature $T = 298.15$ K and a density corresponding to pressure $P =$ 1.0 bar, using the DL_POLY simulation code [44].

The simulations were carried out using 238 anion-cation pairs and 12 water molecules in the central simulation box, corresponding to a 0.048 water mole fraction and resembling the concentration of the experimental study of Fayer and coworkers [41]. The starting structure was generated by using the Packmol software [45]. The density of the system was first determined by performing a simulation in the NPT ensemble. A 5 ns equilibration NPT simulation at $T = 298.15$ K and $P =$ 1.0 bar was initially performed for the liquid mixture. The density of the system was then calculated from a subsequent 5 ns NPT simulation. Afterwards, using a starting structure corresponding to the precalculated density, a further 5 ns NVT simulation was performed to equilibrate the system in the canonical ensemble and the structural and dynamic properties of the system were evaluated by performing another subsequent 5 ns NVT simulation, after the initial 10 ns equilibration. Note that test runs on pure [Emim$^+$][TF$_2$N$^-$] have revealed that this total 15 ns simulation time is more than enough to ensure that the simulated system has reached equilibrium, as well as to ensure that the relaxation processes taking place in the liquid can be sufficiently sampled in the time scale of the simulations reported in the present study. The equations of motion were integrated using a leapfrog-type Verlet algorithm [46] and the integration time step was set to 0.5 fs. The Nose-Hoover thermostat [47] and barostat [48] with temperature and pressure relaxation times of 0.5 and 1.0 ps, respectively, were used to constrain the temperature and the pressure during the simulations. The chemical structure (and atomic labelling) of the [Emim$^+$] cation and the [TF$_2$N$^-$] anion is indicated in Fig. 1. The force field employed for the ionic liquid in the simulations was adopted from the work of Van-Oanh et al. [49] (see Supporting Information of Ref. [49]), whereas the SPC/E model [50] has been employed for water. The intermolecular interactions are represented as pair wise additive with site-site Lennard-Jones plus Coulomb interactions. Intramolecular vibrations have been represented in terms of harmonic bond stretching and angle bending, as well as a cosine series for dihedral angle internal rotations. The parameters for the Lennard-Jones and the intramolecular interactions corresponding to the cation have been adopted from the force field proposed by Maginn and coworkers [38,51] and partial charges were determined using the CHELPG algorithm on the electron densities calculated at B3LYP/6311-G* level [49]. Regarding the interactions in the anion, the parameters have been adopted from the work of Lopes and Padua [52]. The reason why we selected this particular force field in our study, is because in Ref. 49 it has been systematically presented that this particular combination provides

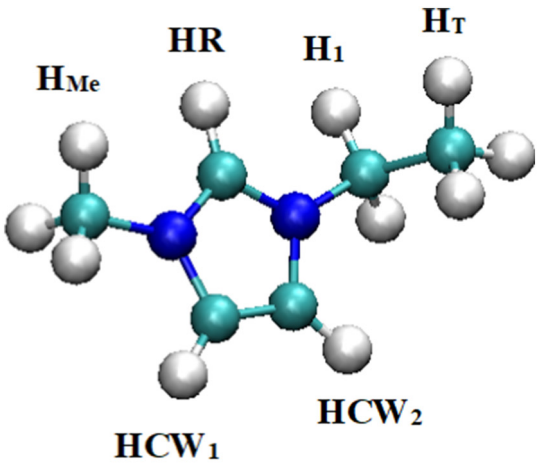

Fig. 1. Chemical structure and atomic labelling of the [Emim$^+$] cation and the [TF$_2$N$^-$] anion.

a very good description of the dynamic and transport properties of the ILs under investigation. The intramolecular geometry of water was constrained using a modified version of the SHAKE algorithm [53,54]. A cut-off radius of 12.0 Å has been applied for all Lennard-Jones interactions and long-range corrections have been also taken into account. To account for the long-range electrostatic interactions the standard Ewald summation technique has been used.

Additional NVT simulations were then performed for HOD in [$Emim^+$][TF_2N^-] at exactly the same composition and density, using the last configuration of the simulations of water in the IL as the starting point and substituting one hydrogen atom with a deuterium. The same force fields have been employed in the simulations. The system was again equilibrated for 5 ns and the system properties were obtained by a subsequent NVT 5 ns run. All the technical details of the simulations have been kept the same as in the case of H_2O in [$Emim^+$][TF_2N^-].

3. Results and discussion

3.1. Local intermolecular structure

The local intermolecular structure in the mixture has been studied in terms of the corresponding center of mass (com) and atomic pair radial distribution functions (rdfs). The calculated com-com rdfs are depicted in Fig. 2. The existence of significant long-range structural correlations is clearly reflected on the shape of these rdfs, which tend to approach a constant value of one at distances in the range of about 25 Å. The first minima of the anion-cation, anion-anion and cation-cation com-com rdfs, which characterize the size of the corresponding solvation shells, are located at 9.15, 12.45 and 12.65 Å, respectively. In the case of the anion-water and cation-water com-com rdfs, the first solvation shell is located at 6.05 and 7.05 Å, respectively. Due to the much small volume of the water solutes, the first minimum of the water-water rdf is shifted at smaller intermolecular distances and it is located at 3.95 Å, exhibiting high intensity. However, the first shell coordination number of water cosolvents around a central water molecule is only 0.1, indicating that although the water-water interactions can be strong, water hydrogen bonded dimers are not frequently observed due to the small concentration of water in the mixture. The smaller volumes of the first solvation shell for the anion-water, cation-water and water-water com-com rdfs in comparison with the ion-ion ones clearly indicate that water molecules interpenetrate the ionic structural networks of the IL and interact with the anions and the cations of the liquid.

The preferential interactions of the water molecules with the different interaction sites of the anions and cations of the IL can be reflected on the shape of the calculated atom-atom rdfs. Particular attention has been paid on the HB interactions between the water molecules and the HB donor or acceptor atoms of the ions. More specifically the fluorine, oxygen and nitrogen atoms of the TF_2N^- anion can act as HB acceptors in order to form hydrogen bonds with the hydrogen atoms of the water molecules. On the other hand, the hydrogen atoms of the imidazolium ring and the alkyl tails of the $Emim^+$ cation can act as hydrogen bond donors in order to form hydrogen bonds with the oxygen atoms of the water molecules. The atom-atom rdfs which are more closely related to the possible formation of hydrogen bonds between the water molecules and the anions and cations of the IL are presented in Fig. 3. From this figure it might be clearly observed that the dominating interactions between the water molecules and the ions are the interactions between the oxygen atoms of the TF_2N^- anion and the hydrogen atoms of the water molecules. The O-H_w rdf exhibits a high intensity peak located at 1.75 Å, followed by a low intensity minimum at 2.55 Å, indicating the existence of HB interactions between these pairs of atoms. The N-H_w rdf exhibits a weak low-intensity shoulder at around 2.55 Å, followed by a peak located at 4.15 Å and a minimum at 4.75 Å and the F-H_w rdf exhibits also a weak shoulder located around 2.55 Å. These are clear indications that the O_{An}…H_w hydrogen bonds are the most pronounced HB interactions between the water molecules

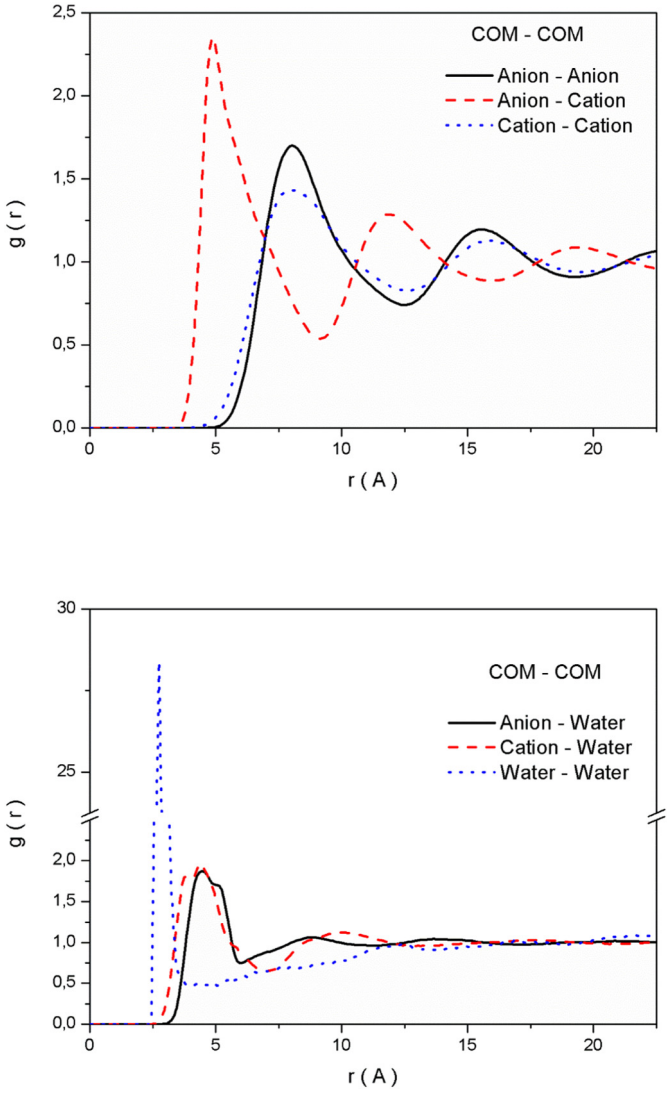

Fig. 2. Calculated com-com rdfs for all the pair combinations involving the ionic liquid's cations, anions and water molecules.

and the TF_2N^-. Using the cut-off distance of 2.55 Å, the calculated coordination number of TF_2N^- oxygen atoms around each water hydrogen atom is 0.93. The coordination numbers of TF_2N^- nitrogen and fluorine atoms around each water hydrogen atom for the same cut-off distance are 0.02 and 0.11, respectively. Although this distance cut-off cannot be considered as a HB definition, it can provide relative trends regarding the HB interactions among between the water molecules and the IL anions and cations. This can be done simply by comparing the coordination numbers corresponding to the pairs which are related to this kind of interactions among the water molecules and the acceptor and donor atoms of the anions and cations, respectively. Summing up all these average coordination numbers, we can see that the average number of the different HB acceptor atoms of each anion around each individual water hydrogen atom is 1.06. Therefore, the corresponding average coordination number of the different HB acceptor atoms of each anion around each water molecule is 2.12.

Regarding the interactions of the different hydrogen atoms of the $Emim^+$ cation with the oxygen atoms of the water molecules, the most pronounced interactions are those between the hydrogen atoms of the imidazolium ring and the water oxygen atoms, as it can be seen in Fig. 3. The HR-O_w rdf exhibits a high intensity peak located at 2.05 Å, followed by a minimum at 3.35 Å. The corresponding first peak locations for each one of the HCW_1-O_w and HCW_2-O_w rdfs are 2.45 and 2.35

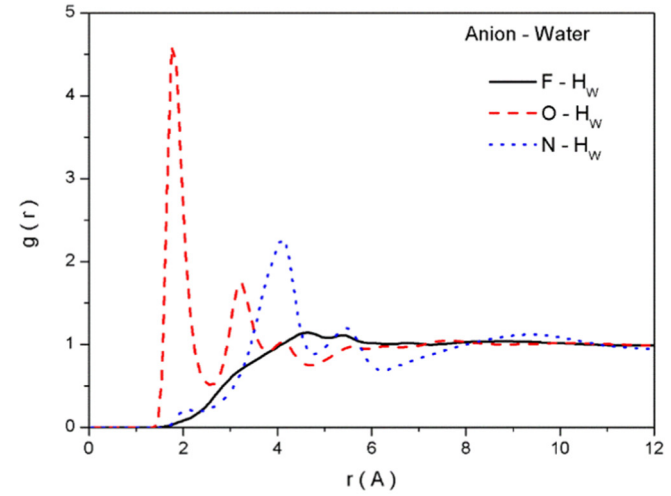

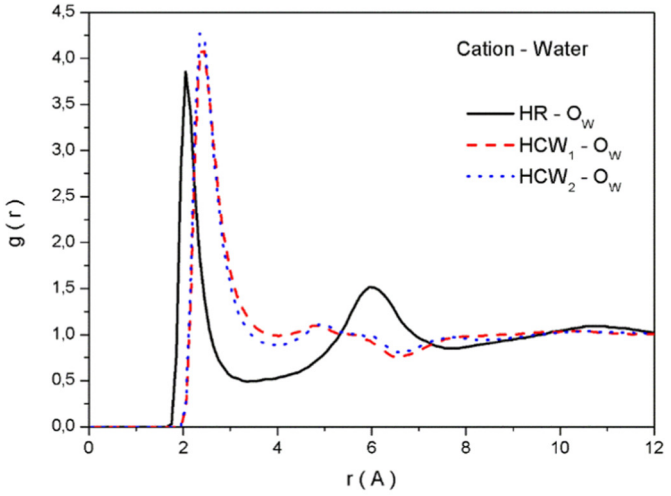

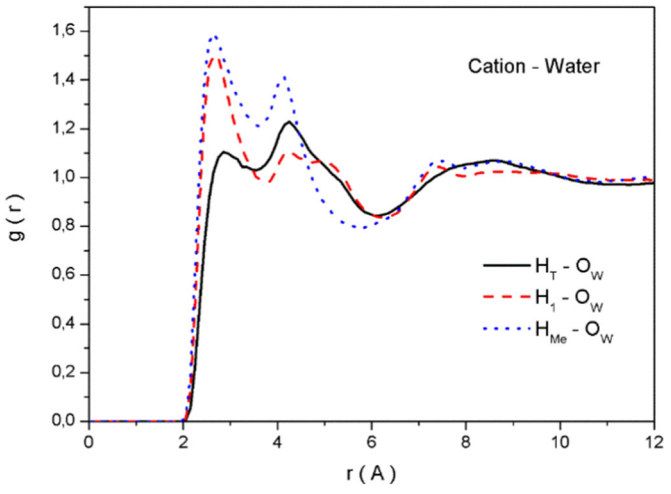

Fig. 3. Calculated atom-atom rdfs corresponding to pairs exhibiting potential hydrogen bonding interactions.

Å, whereas their first minima are located at 4.05 and 3.85 Å, respectively. Using the cut-off distance of 2.55 Å, previously used to describe the water-anion HB interactions, the calculated coordination numbers for the pairs O_w…HR, O_w…HCW_1 and O_w…HCW_2, estimated per each water oxygen atom, are 0.24, 0.27 and 0.28, respectively. In the case of the methyl and ethyl hydrogen atoms of the cation, the intensities of the first peak of the corresponding rdfs are significantly lower, signifying a preferential interaction of the water molecules with the hydrogen atoms of the imidazolium ring. Using again the same cut-off distance of 2.55 Å, the estimated coordination numbers corresponding to the O_w…H_{Me}, O_w…H_1 and O_w…H_T pairs were 0.25, 0.15 and 0.13, respectively. Summing up again all these coordination numbers, we estimate that the total average coordination number of the HB donor hydrogen atoms of the $Emim^+$ cations around each water molecule is 1.3. This is a clear quantitative indication that there is a slight preference of the water molecules to interact with the HB acceptor atoms of the TF_2N^- anions, rather than with the HB donor atoms of the $Emim^+$ cations. The fact that anion-water atom-atom rdfs exhibit their first minima at smaller interatomic distances in comparison with the cation-water ones further supports this argument. This finding is also in agreement with the findings of the experimental studies of Fayer and coworkers [41].

3.2. Local residence dynamics

The dynamics related to local structural changes in the mixture have been investigated in terms of selected pair interatomic residence dynamics. Particular attention has been paid to the water-anion and water-cation interactions. The pair residence dynamics time correlation function (tcf) for a selected couple of atoms i and j is defined as follows [55,56]:

$$C_{res}(t) = \frac{\langle n_{ij}(0) \cdot n_{ij}(t) \rangle_{t^*}}{\langle n_{ij}(0)^2 \rangle} \quad (1)$$

where $n_{ij}(t) = 1$ if a specific atom j is within a pre-defined cut-off distance of a second atom i at times 0 and t, and the atom j has only left the cut-off sphere for a period shorter than t^* during the time interval [0,t], otherwise $n_{ij}(t) = 0$.

The corresponding residence time is defined according to the following relation:

$$\tau_{res} = \int_0^\infty C_{res}(t) \cdot dt \quad (2)$$

According to this definition, $C_{res}(t)$ depends on the selection of the parameter t^*, and two limiting cases arise:

a) $t^* = 0$, which corresponds to atom j remaining in the solvation cut-off sphere of atom I continuously for the whole-time interval [0, t]. In this case we define the continuous residence time correlation function $C_{res}{}^C(t)$ and the corresponding continuous residence lifetime $\tau_{res}{}^C$.

b) $t^* = \infty$, where the intermittent presence of atom j in the solvation cut-off sphere of atom I at time t is investigated, regardless of the number of exits and entrances of this atom into the cut-off sphere during the time interval [0, t]. In this case we define intermittent residence correlation function $C_{res}{}^I(t)$ and the corresponding intermittent residence lifetime $\tau_{res}{}^I$.

In the present treatment we focused on the calculation of the intermittent pair residence dynamics, using a reference radial cut-off of 2.55 Å. The intermittent dynamics are more related to the structural

relaxation processes in liquids taking place at longer time scales and for this reason they have been preferred to be studied in the present treatment. This cut-off corresponds to the one used to estimate the number of hydrogen bonds formed between the water and the different atoms of the anions and the cations, as previously mentioned. Additional tests using a longer cut-off distance of 4.0 Å were also performed. This cut-off distance is quite similar to the largest first solvation shell radius among the pairs taken into account in our studies and it was used in order to investigate the length scale effects upon these dynamics.

In the previous section we revealed that the O_{An}…H_w interactions are the most pronounced between the water molecules and the TF_2N^- anion. On the other hand, the HR…O_w, HCW_1…O_w and HCW_2…O_w interactions are the most pronounced between the water molecules and the $Emim^+$ cation. For this reason, we focused on the investigation of the intermittent pair residence dynamics for these specific atom pairs. The intermittent residence tcfs $C_{res}{}^{I}(t)$ for these pairs and for the two cut-off distances of 2.55 and 4.0 Å are depicted in Fig. 4 and the corresponding intermittent residence lifetimes $\tau_{res}{}^{I}$ are presented in Table 1.

From the values reported in Table 1 we can say that at short interatomic distances, where HB interactions are the dominating ones, the lifetimes corresponding to the HR…O_w and O_{An}…H_w pairs (53.8 and 45.0 ps, respectively) are significantly longer in comparison with the ones corresponding to the HCW_1…O_w and HCW_2…O_w pairs. However, when increasing the cut-off distance, the lifetimes corresponding to the HCW_1…O_w and HCW_2…O_w pairs are much more increased and they become slightly longer in comparison with the HR…O_w one, with the lifetimes corresponding to HCW_2…O_w and the O_{An}…H_w pairs being the longest ones (111.9 and 105.9 ps, respectively). Such an observation signifies that when the hydrogen bonds between the water and the different binding sites of ions break, the water molecules are located in the region between the anions and the cations and they diffuse until they form a new hydrogen bond with another atom of either the anion or the cation.

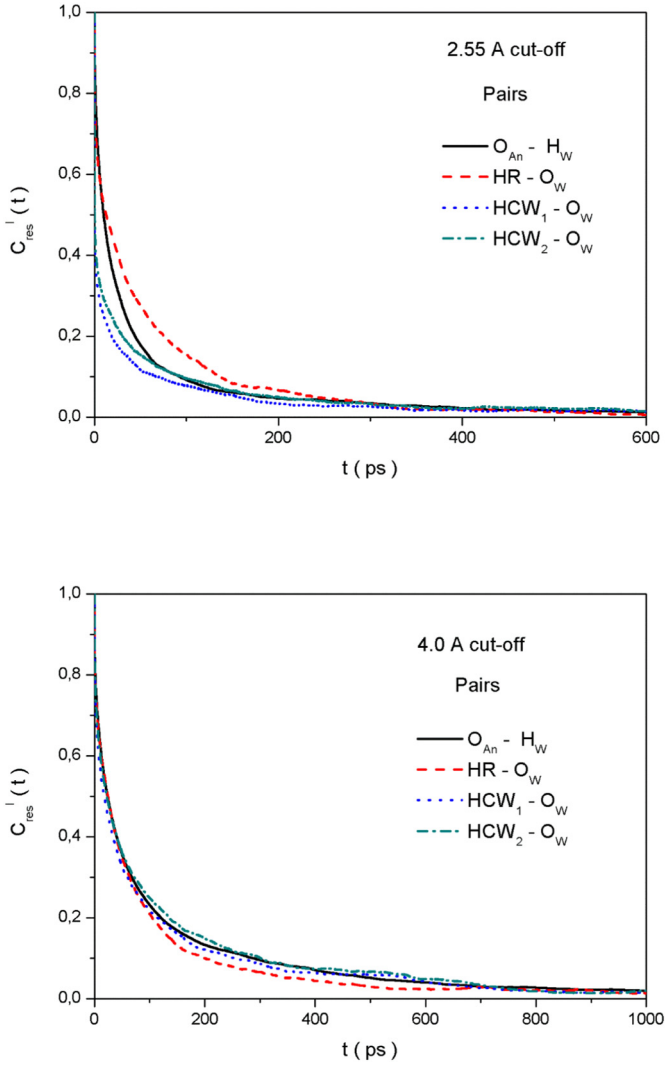

Fig. 4. Calculated intermittent residence tcfs corresponding to two different cut-off distances of 2.55 and 4.0 Å.

3.3. Translational dynamics

The translational dynamics of the water molecules and the cations and anions of the IL have been investigated in terms of the com velocity tcfs:

$$C_v{}^{i}(t) = \frac{\left\langle \vec{v}_i(0) \cdot \vec{v}_i(t) \right\rangle}{\left\langle \vec{v}_i(0)^2 \right\rangle} \tag{3}$$

with the associated spectral densities, $S_v{}^{i}(\omega)$, calculated by performing a Fourier transform

$$S_v{}^{i}(\omega) = \int_0^\infty \cos(\omega \cdot t) \cdot C_v{}^{i}(t) \cdot dt \tag{4}$$

Here, the $S_v{}^{i}(\omega)$ have been calculated by numerical integration using a Bode rule and also applying a Hanning window. As pointed out in recent reviews [57], in this way the intermolecular vibrational dynamics and rattling dynamics of ions within a temporary cage made of neighboring ions can be studied in an efficient way. The calculated com velocity tcfs and corresponding normalized $(S_v{}^{i}(\omega)/S_v{}^{i}(0))$ spectral densities are presented in Fig. 5. From this figure it can be clearly seen that the translational dynamics of the anions are slower in comparison with the dynamics of the cations and especially with the water molecules. The com velocity tcf of the anions exhibits a negative minimum at 0.68 ps and loses any kind of correlation at about 2 ps. This process is much faster is the case of water molecules, where the com velocity tcf exhibits a very fast initial decay and a negative minimum at 0.12 ps and reaches the zero value at about 0.6 ps. Similarly, the com velocity tcf of the cations exhibits a fast initial decay, with a negative minimum observed at 0.26 ps, and finally reaches the zero value at about 1.5 ps. All these features clearly indicate the existence of more pronounced low frequency translational motions in the case of water molecules. This is more clearly reflected on the shape of the corresponding spectral densities, particularly in the low-frequency part of the spectra. In the case of the anions, a peak located at 16 cm^{-1} has been observed. This peak has been shifted to the higher frequency of 35 cm^{-1} in the case of the cation, reflecting the existence of more pronounced cage librations. Finally, in the case of water a first peak at 61 cm^{-1} is observed, followed by another peak located at 125 cm^{-1}. The first peak reflects more the cage effects, whereas the second band could be interpreted as more closely related to the interactions of hydrogen bonded dimers [58]. These findings are clear manifestations of the faster, low frequency, translational modes of water molecules in the liquid mixture, due to its strong interactions with the anions and the cations of the IL.

The translational self-diffusion coefficients of the cations, anions and water molecules were also calculated in the present study, by calculating their com mean-square displacements and using the well-known Einstein relation:

$$D = \frac{1}{6} \lim_{t \to \infty} \frac{1}{t} \left\langle \left| \vec{r}_i(0) - \vec{r}_i(t) \right|^2 \right\rangle \tag{5}$$

Table 1
Calculated intermittent residence lifetimes τ_{res}^{I}, corresponding to selected water-anion and water-cation interatomic pairs. The lifetimes have been calculated using two cut-off distances of 2.55 and 4.0 Å.

Pairs	O_{An} - H_w	HR - O_w	HCW_1 - O_w	HCW_2 - O_w
τ_{res}^{I} (ps) ($r_c = 2.55$ Å)	45.0	53.8	30.8	39.9
τ_{res}^{I} (ps) ($r_c = 4.0$ Å)	105.9	94.0	98.8	111.9

The calculated mean square displacements as a function of time are depicted in Fig. 6. From this figure it can be clearly seen that there is about an order of magnitude difference between the mean-square displacements of water molecules and the ions. Indeed, the calculated average self-diffusion coefficients are $4.51 \cdot 10^{-10}$, $0.75 \cdot 10^{-10}$ and $0.50 \cdot 10^{-10}$ m^2/s for the water molecules, cations and anions, respectively. However, the self-diffusion of the water molecules, although almost one order of magnitude higher than the ionic diffusion coefficients, is still one order of magnitude lower in comparison with liquid ambient water, which has an experimentally measured value of $22.99 \cdot 10^{-10}$ m^2/s [59]. On the other hand the calculated values of the ions are quite close to the experimentally reported values [60] for pure $[Emim^+][TF_2N^-]$ at 303 K and ambient pressure, which are $0.62 \cdot 10^{-10}$ and $0.37 \cdot 10^{-10}$ m^2/s for the cation and the anion, respectively. Taking also into account that the small addition of water will reduce the viscosity and increase the diffusion of the IL components, these findings signify a very good agreement between the calculated and experimental self-diffusion values of the cations and anions. Our findings are also in very good agreement with the results reported in the pulse field gradient nuclear magnetic resonance measurements of Yaghini et al. [61] (see fig. 3 in Ref [61]). This agreement further verifies the validity of the force field used in our simulations and it is an additional validation of the trends reported in the present study regarding the translational mobility of each component of the mixed water-IL system.

3.4. Rotational dynamics

Recent studies have underlined the fact that ion reorientations seem to play a significant, but so far mostly overlooked, role for the ionic charge transport in ILs [62]. Interestingly it has been found that the rotation of the dipolar ions opens paths for the passage of other ions, pointing to a revolving-door mechanism [62]. A similar mechanism was previously considered for plastic crystals [63], but, in contrast to these materials, in ILs the centers of the revolving doors can also move translationally [62]. Other recent studies [21] on ILs containing HB tracer molecules have also pointed out that the structural and energetic heterogeneities in these systems are strongly reflected on the mechanisms of rotational relaxation of the solutes. These previous studies pointed out that the rotational relaxation of small HB solutes in ILs is far from ideal with multiple relaxation channels and time scales [21]. Therefore, a more detailed analysis of the dynamics of the different reorientational modes of the cations and anions of ILs, as well as of their cosolvents, becomes indispensable in order to shed more light on the role of rotational motions on the properties of ILs and their mixtures. Rotational dynamics in liquids can be efficiently characterized in terms

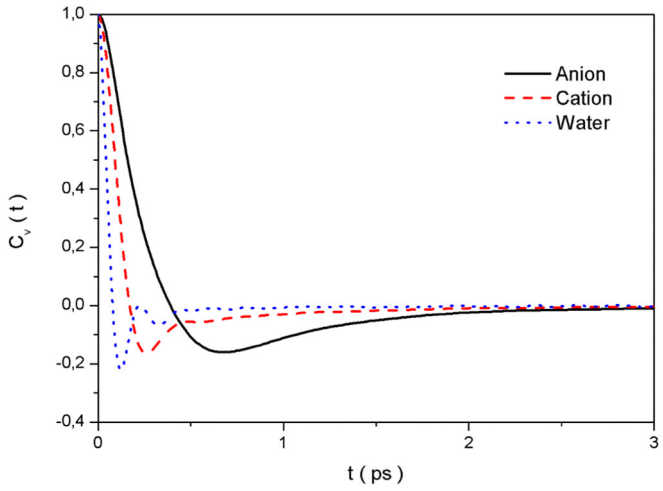

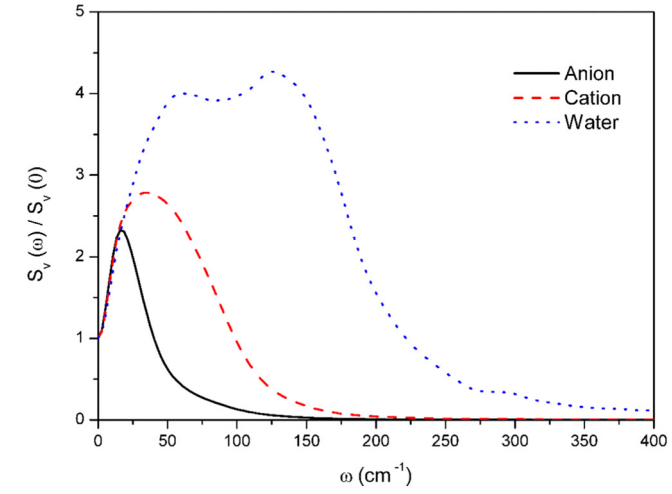

Fig. 5. Calculated com velocity tcfs for the anions, cations and water molecules and corresponding normalized spectral densities.

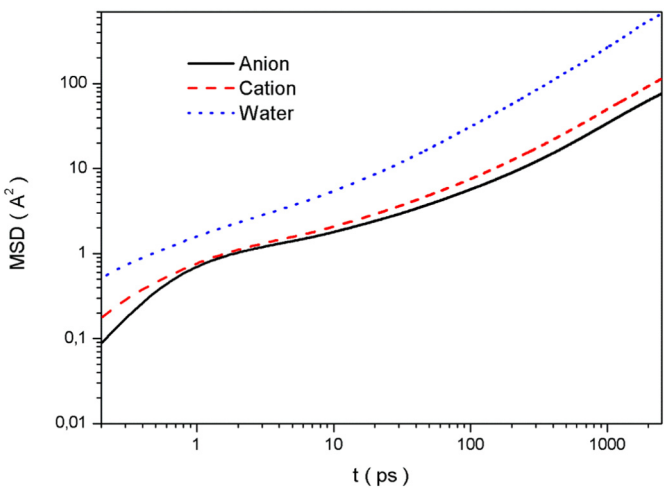

Fig. 6. Calculated time dependence of the translational mean square displacements for the anions, cations and water molecules.

of the well-known Legendre reorientational tcfs of adapted intramolecular vectors

$$C_{\ell R}(t) = P_\ell\left\langle \vec{u_i}(0)\cdot\vec{u_i}(t)\right\rangle \quad (6)$$

Here, $\vec{u_i}$ is a normalized vector associated to molecule i, and P_ℓ is a Legendre polynomial of order ℓ. In the present study the end-to-end intramolecular vectors of the anions and cations were selected to be studied, together with the vectors whose motions are closely related to the formation of strong hydrogen bonds with the water molecules. In the case of the anion we selected the S=O vector and in the case of the cation the CR-HR one, since the oxygen atoms of the anions and the HR hydrogen of the imidazolium ring of the cations form the strongest hydrogen bonds with the water molecules. In the case of the water molecules, the reorientation of the O-H vector was studied. The calculated first, second and third order Legendre reorientational tcfs for all these vectors are presented in Figs. 7–9. The corresponding reorientational correlation times have been calculated using the relation:

$$\tau_{\ell R} = \int_0^\infty C_{\ell R}(t)\cdot dt \quad (7)$$

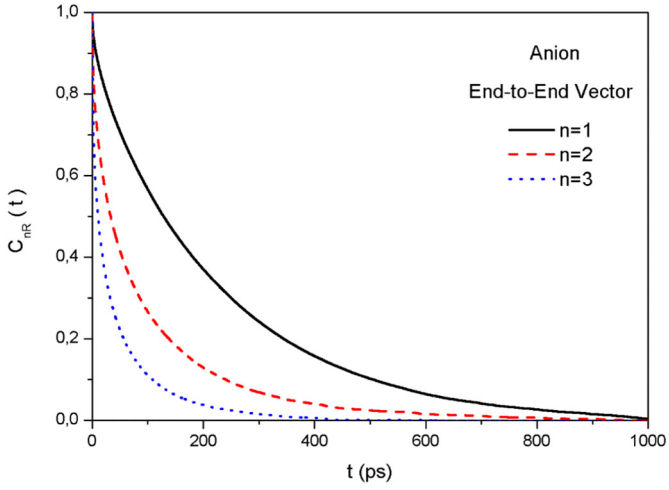

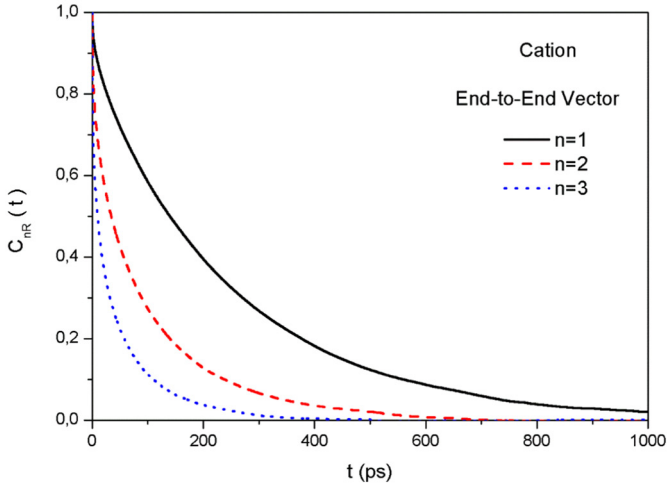

Fig. 7. Calculated first, second and third order Legendre reorientational tcfs for the end-to-end vectors of the ionic liquid's anions and cations.

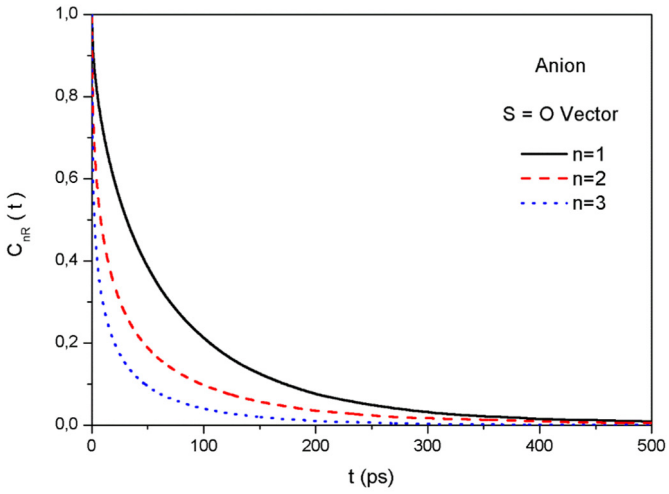

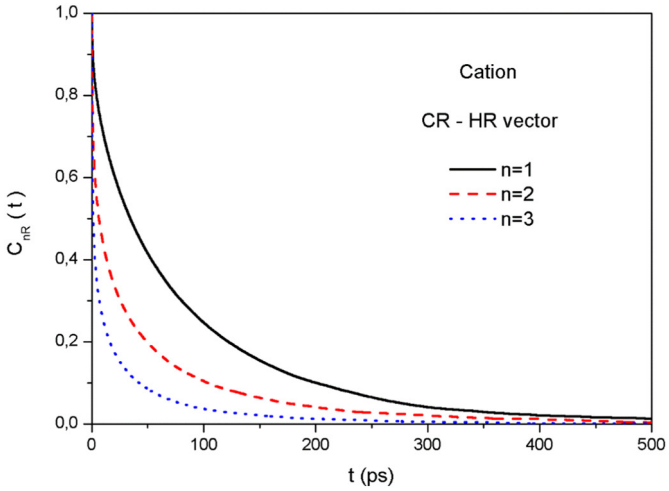

Fig. 8. Calculated first, second and third order Legendre reorientational tcfs for the S=O and CR-HR vectors of the ionic liquid's anions and cations, respectively.

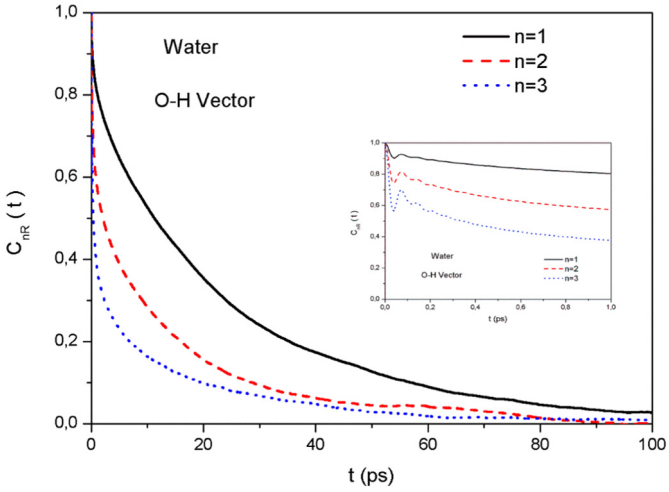

Fig. 9. Calculated first, second and third order Legendre reorientational tcfs for the O-H vector of the water molecules. The short-time decay of the tcfs is displayed in the inset figure.

The calculated values of the Legendre reorientational correlation times for the several vectors taken into account are also presented in Table 2. From Figs. 7–9 and Table 2 it can be clearly observed that the reorientation of the water molecules is much faster in comparison with the anions and the cations. The calculated first-order Legendre reorientational correlation time for the O-H vector of water is 21.3 ps, whereas the corresponding correlation times of the S=O vector of the anion and the CR-HR vector of the cation are 66.0 and 74.0 ps, respectively. On the other hand, the reorientation of the end-to-end vectors of the anions and the cations is even slower; the corresponding first-order Legendre reorientational correlation times for the end-to-end vectors of the anions and the cations are about 203 and 224 ps, respectively. This is a clear indication that the reorientational dynamics of the anion and the cation is very anisotropic and the mechanisms of the rotation around different intramolecular axes take place at different time scales. Moreover, there is a very clear deviation of the calculated Legendre reorientational correlation times from the trends expected when using the Debye diffusion model of reorientational relaxation [64,65] ($\tau_{1R} = 3 \cdot \tau_{2R}$, $\tau_{1R} = 6 \cdot \tau_{3R}$). This finding indicates that the reorientational dynamics of the investigated vectors cannot be described in terms of a diffusive model. Interestingly, the calculated second-order Legendre reorientational correlation time for the CR-HR vector of the cation (36.1 ps) has found to be in good agreement with the value of 42.8 ps measured for pure [$Emim^+$][TF_2N^-] at 300 K and ambient pressure using ^2H magnetic relaxation experiments [66].

In order to have a more complete picture of the reorientation mechanisms, we also calculated the self, angular Van Hove correlation functions [67,68] for the O-H, S=O and the CR-HR vectors using the following equation:

$$G(\theta,t) = \frac{2}{N \cdot \sin\theta} \sum_{i=1}^{N} \left\langle \delta\left[\theta - \cos^{-1}\left(\vec{u}_i(0) \cdot \vec{u}_i(t)\right)\right]\right\rangle \quad (8)$$

The calculated $1/2 \cdot \sin\theta \cdot G(\theta,t)$ functions for three characteristic different time scales, corresponding to $t = 0.5$, 5.0 and 50.0 ps, are presented in Fig. 10. The faster reorientation of the O-H vector of the water molecules is reflected on the shape of these functions. The peak of the distribution at short-time scales (0.5 and 5.0 ps) is located at larger angular values in comparison with the functions corresponding to the S=O and the CR-HR vectors. Moreover, the distribution function corresponding to the O-H vector decays to zero at much larger angular values. At the larger time scale of 50 ps even the shape of the distributions is different, with the distribution corresponding to the O-H vector being much broader in comparison with the other two, which exhibit clear sharper peaks at small angular values. This difference clearly indicates that the rotation of the O-H vector of water molecules is significantly faster.

The difference in the rotational dynamic behavior of water molecules and the different vectors of the anions and cations of the IL can be additionally highlighted by calculating the angular mean-squared displacements [69–71] together with the corresponding rotational diffusion coefficient, through the Einstein relation:

$$D_R = \lim_{t\to\infty} \frac{1}{4t} \left\langle \Delta\phi^2(t) \right\rangle \quad (9)$$

Table 2
Calculated values of the first-, second- and third-order Legendre reorientational correlation times for selected intramolecular vectors of the ionic liquid's anions and cations and for the O-H vector of water.

Vectors	End-to-end (Anion)	End-to-end (Cation)	S=O (Anion)	CR-HR (Cation)	O-H (Water)
τ_{1R} (ps)	202.9	224.4	66.0	74.0	21.3
τ_{2R} (ps)	86.3	84.3	34.7	36.1	10.2
τ_{3R} (ps)	37.4	36.9	16.7	15.3	6.3

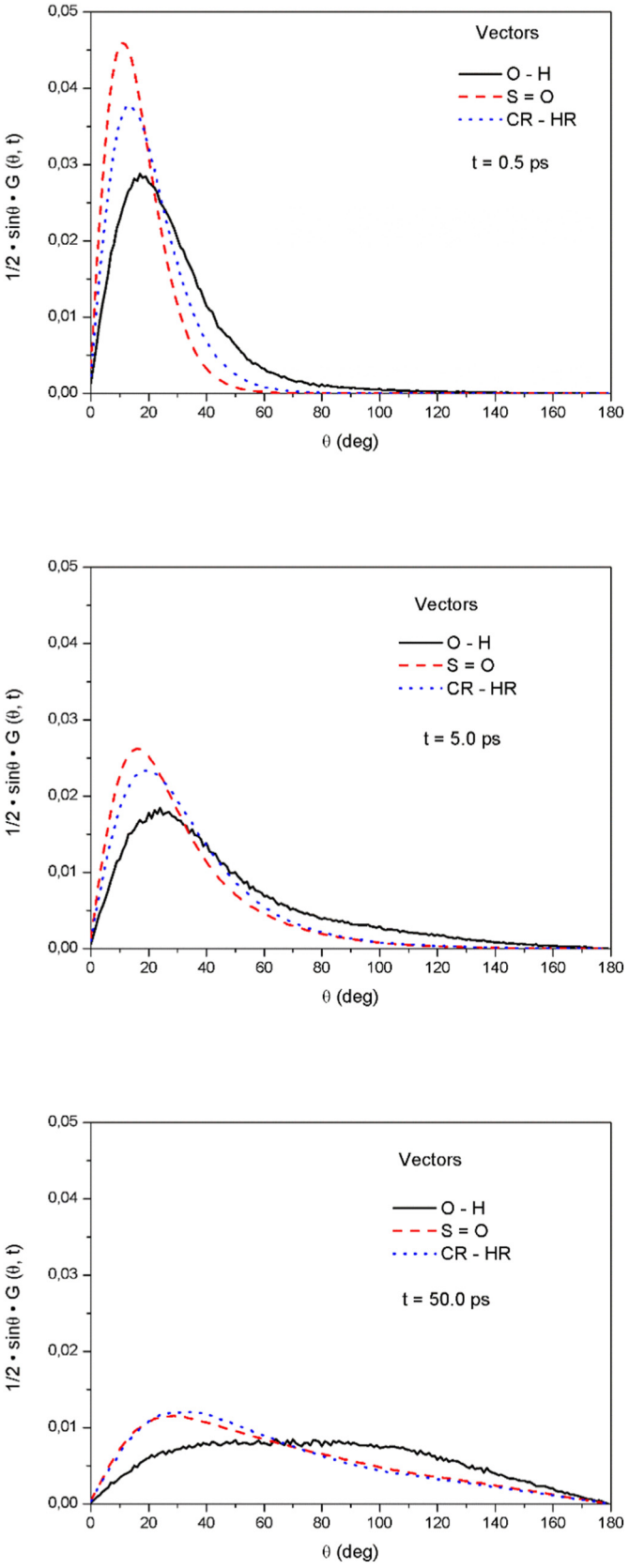

Fig. 10. The calculated $1/2 \cdot \sin\theta \cdot G(\theta,t)$ probability distribution functions for the O-H, S=O and CR-HR of the water molecules, anions, cations, respectively. The distribution functions correspond to three characteristic different time scales, at $t = 0.5$, 5.0 and 50.0 ps.

The time-dependence of the calculated average mean-squared angular displacements for the O-H vector of the water molecules and the ionic end-to-end vectors, as well as the S=O vector of the anion and the CR-HR vector of the cation are presented in Fig. 11. The angular mean square displacements of specific intramolecular vectors provide a straightforward way to calculate the rotational diffusion of these vectors, whereas in the case of the Legendre reorientational correlation functions the rotational diffusion can be estimated only by using specific models for the reorientational relaxation mechanisms. The calculated values of the rotational diffusion of each selected intramolecular bond vector also provide an alternative quantitative way of observing the anisotropy of the rotational motions in the liquid. From Fig. 11 it can be clearly seen that at the long-time scale the mean square angular displacement of the O-H vector of water is about one order of magnitude higher than the ones corresponding to the end-to-end vectors of the IL anions and cations, which are almost identical. This is also reflected on the calculated rotational diffusion coefficients. The value obtained for the O-H vector of water is $D_R = 68.0 \cdot 10^9$ rad^2/s, whereas the values corresponding to the end-to-end vectors of the anion and the cation are $3.72 \cdot 10^9$ rad^2/s and $3.68 \cdot 10^9$ rad^2/s, respectively. The calculated rotational diffusion values corresponding to the S=O and the CR-HR vectors are $11.66 \cdot 10^9$ and $13.96 \cdot 10^9$ rad^2/s, respectively. All these findings clearly indicate the much faster rotation of water molecules in comparison with the IL anions and cations, as well as the slightly faster rotation of the $Emim^+$ cations in comparison with the $[TF_2N^-]$ anions.

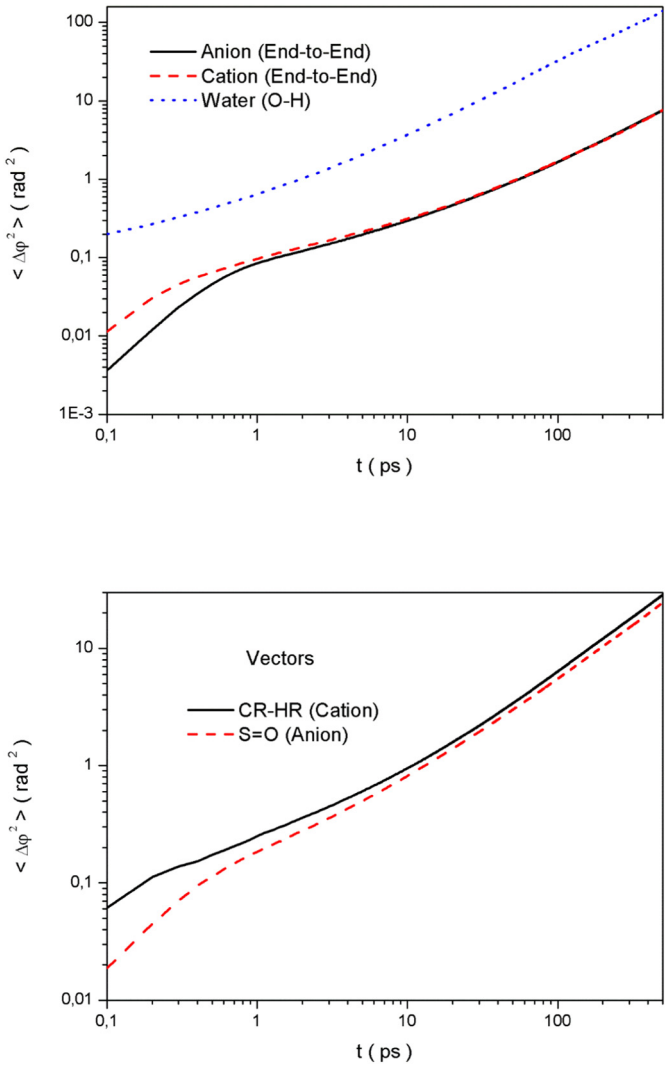

Fig. 11. Calculated time dependence of the angular mean-squared displacements for the O-H vector of the water molecules and the ionic end-to-end vectors, as well as the S=O vector of the anion and the CR-HR vector of the cation.

As mentioned in the introduction, quite recently Fayer and coworkers [41] investigated the dynamics of a series of small HB tracer molecules (water, methanol and ethanol) diluted to low concentration in $[Emim^+][TF_2N^-]$ by using 2D IR vibrational echo spectroscopy and polarization resolved pump-probe experiments on the deuterated hydroxyl (O–D) stretching mode of each of the solutes. From these experiments the orientational correlation functions for these systems were obtained by measuring the orientational anisotropy $r(t)$, which can be directly related to the second-order Legendre reorientational tcf [41,72,73]:

$$r(t) = \frac{2}{5} \cdot C_{2R}(t) \tag{10}$$

Using this relation, the orientational anisotropy $r(t)$ can be directly calculated and compared with the experimental results. To be more precise in the comparison with the experiment, apart from simulating the $H_2O/[Emim^+][TF_2N^-]$ mixture, we also simulated the $HOD/[Emim^+][TF_2N^-]$ mixture at exactly the same composition and density with the $H_2O/[Emim^+][TF_2N^-]$ mixture. In this way the orientational anisotropy $r(t)$ corresponding to the O-D vector could be directly related to the experimental one and could also be compared to the one obtained for the O-H vector of H_2O. The calculated orientational anisotropy for both the O-D vector of HOD and the O-H vector of H_2O are presented in Fig. 12, together with the experimental data obtained at several representative pump-probe frequencies. The results obtained have revealed a good agreement between the calculated and the experimental orientational anisotropy $r(t)$ corresponding to the O-D vector, with the best agreement obtained with the experimental data corresponding to the pump-probe frequency of 2659 cm^{-1}. Interestingly, the decay of the calculated orientational anisotropy for the O-D vector exhibits some differences with the one corresponding to the O-H vector of H_2O. This finding further motivated us to study the isotopic effects on the different rotational motions of the water molecules and to compare the calculated first- and second-order Legendre reorientational tcfs of the O-D vector of HOD with the ones corresponding to the O-H vectors of HOD and H_2O. The calculated functions, presented in Fig. 13, exhibit some differences which are more pronounced in the case of the first-order Legendre reorientational tcfs. The differences are also reflected on the

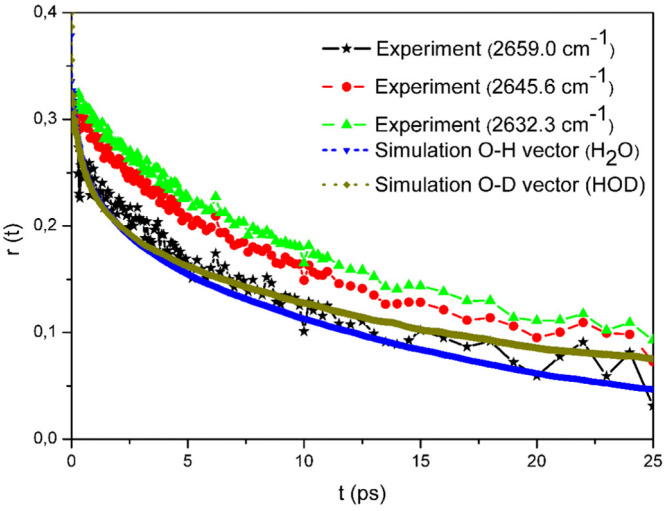

Fig. 12. Calculated orientational anisotropy r(t) for both the O-D vector of HOD and the O-H vector of H_2O. The r(t) functions obtained by the simulations are presented together with the experimental ones (black, red and green curves), reported by Fayer and coworkers [41], corresponding to the O-D vector of HOD and obtained at several representative pump-probe frequencies.

calculated reorientational correlation time. The calculated first-order Legendre reorientational correlation times τ_{1R} corresponding to the O-D vector of HOD and the O-H vectors of HOD and H_2O are 26.6, 21.9 and 21.3 ps, respectively. The corresponding second-order Legendre reorientational correlation times τ_{2R} for the previously mentioned vectors have been found to be 11.1 ps (O-D vector of HOD), 10.4 ps (O-H vector of HOD) and 10.2 ps (O-H vector of H_2O), respectively. At this point it should be mentioned that the short-time scale behavior of the Legendre reorientational tcfs, in the time scale 0–0.3 ps, is different. This can be clearly seen in the inset pictures in Fig. 13, where the location of the local minima and maxima, closely related to the local structural changes around the water molecules due to the breaking and formation of hydrogen bonds, is different in the case of each vector. This finding indicates the existence of non-negligible isotope effects on the short-time scale reorientational dynamics of the H_2O and HOD molecules.

However, the calculated angular mean square displacements of these vectors, presented in Fig. 14, especially at long-time scales exhibit a different, very interesting behavior. At short-time scales, as depicted in the inset of Fig. 13, the angular mean square displacement follows the trend: O-H (H_2O) > O-H (HOD) > O-D (HOD). This behavior is consistent with the relative trends in the moment of inertia of the molecules. However, at long-time scales this trend is reversed and the angular mean-square displacement of the O-D vector is about 2 times higher than the one obtained for the O-H vector of H_2O. Interestingly, we can actually identify several different time scales describing the time dependence of the angular mean square displacement of the investigated intramolecular vectors. As mentioned before, at very short time scales (0–0.25 ps) the angular mean square displacement $\langle \Delta\phi^2(t) \rangle$ of the O-H vector of water molecules is higher, probably due to the somewhat lower moment of inertia of H_2O in comparison with HOD. This also comes in agreement with the short-time scale behavior of the Legendre reorientational tcfs, presented in Fig. 12, where the location of the local extrema in the case of the tcfs calculated for the O-H vector of H_2O is observed at slightly shorter time scales. Then in the time scale of about 0.25–20 ps the rotational diffusive behavior of all the investigated vectors is similar and then during the time scale 20–100 ps the $\langle \Delta\phi^2(t) \rangle$ of the O-D vector start to become slightly higher. However, this difference becomes significantly more pronounced at time scales longer than about 100 ps, where the rotation of the O-D vector becomes much faster at this specific time scale, followed by the O-H vector of HOD and finally by the O-H vector of H_2O. Actually, this long-time scale behavior can be interpreted on the basis of the conclusions of previous studies devoted to the use of vibrational spectroscopy as a probe of the structure and dynamics in liquid water [73]. According to these studies, on longer time scales the reorientational dynamics require rearrangements of the water network [74,75]. In this regime the dynamics are no longer determined by the moment of inertia but instead are governed by the relative motions of the water molecules and, in particular, by the dynamics of H-bond breaking and reformation. Similarly, in mixtures with ILs the reorientational dynamics at longer time scales should be mainly controlled by the water-IL interactions and the collective dynamic processes related to the structural and dynamic changes of the structural network around the water molecules. Previous studies by Margulis and coworkers [20] and Samios and coworkers [76,77] have also indicated that the dynamics of the motions of small penetrant molecules in slow-moving IL and polymer matrices can indeed take place in different time scales and the corresponding relaxation mechanisms are mainly controlled by local caging dynamics and molecular hopping events.

By inspecting the behavior of the first-order Legendre reorientational tcfs, it can be observed that their decay in the time scale 0.25–20 ps is very similar. Moreover, the time scale around 20–25 ps is quite similar to the value of the relaxation time of these correlation functions. After this specific time scale, the rotation of the H_2O and HOD molecules should be mainly determined by the interaction of the water molecules with the IL. To have a more complete picture

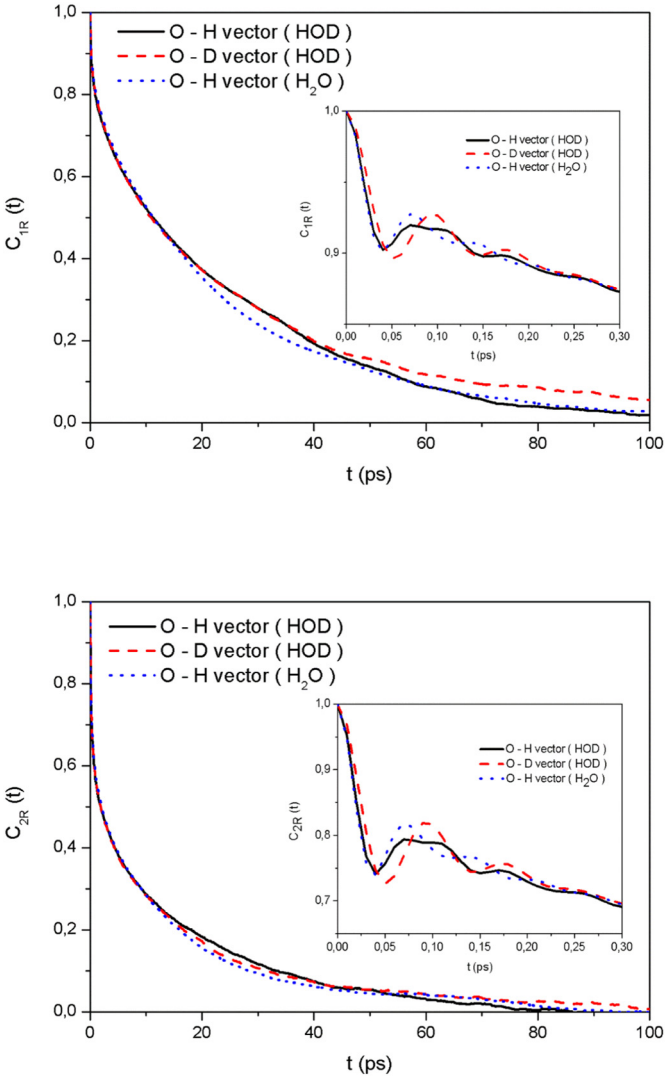

Fig. 13. Calculated first- and second-order Legendre reorientational tcfs of the O-D vector of HOD, plotted together with the tcfs corresponding to the O-H vectors of HOD and H_2O. The short-time decay of the tcfs is presented in the inset pictures.

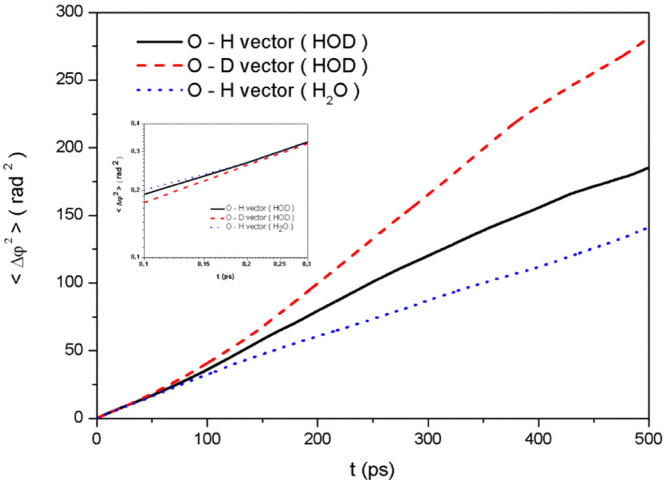

Fig. 14. Calculated time dependence of the angular mean square displacement of the O-D vector of HOD and the O-H vectors of HOD and H_2O.

about these dynamics, the intermittent residence dynamics of the O_{An}…H_w and O_{An}…D pairs in the HOD/IL mixture were additionally studied for the cut-off distances of 2.55 and 4.0 Å, as described in Section B. The obtained residence lifetimes for the O_{An}…H_w pair corresponding to these two cut-off distances are 37.2 and 77.5 ps, respectively. The corresponding values for the O_{An}…D pairs and the two cut-off distances are 36.7 and 77.9 ps, respectively. These values are lower to the corresponding values of 45.0 and 105.9 ps reported for the O_{An}…H_w pairs in the H_2O/IL mixture, signifying the anion-HOD residence dynamics are faster in comparison with the anion-H_2O ones. Similar trends have been also observed for the cation-HOD and cation-H_2O residence dynamics. These differences in the residence lifetimes can provide a reasonable explanation for the appearance of the differences in the calculated $\langle \Delta\phi^2(t) \rangle$ values in the time scale of 20–100 ps and the more pronounced differences at longer-time scales, which are higher in comparison with the lifetimes describing the water-IL interactions at short-range distances (up to 4 Å). All these findings clearly indicate that the rotational dynamics of HOD molecules are highly anisotropic and different in comparison with the corresponding dynamics of H_2O molecules in the investigated mixture.

4. Conclusions

Molecular Dynamics simulations have been employed to investigate the local structural and dynamic properties of low-concentrated water and HOD dissolved in the [$Emim^+$][TF_2N^-] ionic liquid. The calculations have revealed a strong interaction between the oxygen atoms of the anion and the hydrogen atoms of the water molecules and a quite important interaction between the hydrogen atoms of the imidazolium ring with the water oxygen atoms. The translational and rotational diffusion of water molecules is almost one order of magnitude lower in comparison with pure water, but still one order of magnitude higher in comparison with the ionic liquid's anions and cations. The translational diffusion of the anions is lower than the diffusion of the cations, whereas the rotational diffusion is very similar. However, the reorientational dynamics of the anion and the cation is very anisotropic and the mechanisms of the rotation around different intramolecular axes take place at different time scales. The calculated orientational anisotropy of the O-D vector of HOD in the ionic liquid has been found to be in very good agreement with available experimental data [41], showing more pronounced differences with the O-H vector reorientational dynamics at long-time scales. In that regime the dynamics are no longer determined by the moment of inertia, but instead are governed by the relative motions of the water molecules. In particular, the rotational dynamics are mainly controlled by the dynamics of H-bond breaking and reformation between the water and the IL's anions and cations and all the collective dynamic processes related to the structural and dynamic changes of the structural network around the water molecules. Our findings are also in agreement with the conclusions of the experimental studies of Fayer and coworkers [41], who have reported that the dynamics of the hydrogen bond strength fluctuations and orientational relaxation takes place in a variety of time scales, ranging from a few hundred femtoseconds to many tens of picoseconds.

Acknowledgements

The reported simulation studies were carried out using partly the facilities of the Greek High-Performance Computing Center (ARIS supercomputer) of the Greek Research and Technology Network (GRNET) and the computing resources of the Physical Chemistry Laboratory at the Department of Chemistry, National & Kapodistrian University of Athens, Greece. The authors are also very grateful to Dr. P. Kramer and Professor M. Fayer from Stanford University (USA), for providing their experimental data for the orientational anisotropy decay of HOD in the ionic liquid [$Emim^+$][TF_2N^-], obtained by their polarization selective IR pump-probe experiments.

References

[1] M. Freemantle, An Introduction to Ionic Liquids, The Royal Society of Chemistry Publishing, Cambridge UK, 2010.
[2] T. Welton, Room-temperature ionic liquids. Solvents for synthesis and catalysis, Chem. Rev. 99 (1999) 2071.
[3] N.V. Plechkova, K.R. Seddon, Applications of ionic liquids in the chemical industry, Chem. Soc. Rev. 37 (2008) 123–150.
[4] Z. Lei, B. Chen, Y.-M. Koo, D.R. MacFarlane, Introduction: ionic liquids, Chem. Rev. 117 (2017) 6633–6635.
[5] R.D. Rogers, K.R. Seddon, Ionic liquids—solvents of the future? Science 302 (2003) 792–793.
[6] P. Wasserscheid, T. Welton, Ionic Liquids in Synthesis, 2nd Ed Wiley-VCH, 2008.
[7] J.P. Hallett, T. Welton, Room-temperature ionic liquids: solvents for synthesis and catalysis. 2, Chem. Rev. 111 (2011) 3508–3576.
[8] E.W. Castner Jr., C.J. Margulis, M. Maroncelli, J.F. Wishart, Ionic liquids: structure and photochemical reactions, Annu. Rev. Phys. Chem. 62 (2011) 85–105.
[9] M. Gorlov, L. Kloo, Ionic liquid electrolytes for dye-sensitized solar cells, Dalton Trans. 20 (2008) 2655–2666.
[10] V.I. Parvulescu, C. Hardacre, Catalysis in ionic liquids, Chem. Rev. 107 (2007) 2615–2665.
[11] A. Visser, R. Swatloski, W. Reichert, R. Mayton, S. Sheff, A. Wierzbicki, J. Davis, R. Rogers, Task-specific ionic liquids for the extraction of metal ions from aqueous solutions, Chem. Commun. 0 (2001) 135–136.
[12] M. Freemantle, Ionic liquids may boost clean technology development, Chem. Eng. News 76 (1998) 32–37.
[13] Z.L. Terranova, S.A. Corcelli, Molecular dynamics investigation of the vibrational spectroscopy of isolated water in an ionic liquid, J. Phys. Chem. B 118 (2014) 8264–8272.
[14] J. Carrete, M. García, J.R. Rodríguez, O. Cabeza, L.M. Varela, Theoretical model for moisture adsorption on ionic liquids: a modified Brunauer–Emmet–Teller isotherm approach, Fluid Phase Equilib. 301 (2011) 118–122.
[15] S. Cuadrado-Prado, M. Domínguez-Pérez, E. Rilo, S. García-Garabal, L. Segade, C. Franjo, O. Cabeza, Experimental measurement of the hygroscopic grade on eight imidazolium based ionic liquids, Fluid Phase Equilib. 278 (2009) 36–40.
[16] L.E. Ficke, J.F. Brennecke, Interactions of ionic liquids and water, J. Phys. Chem. B 114 (2010) 10496–10501.
[17] A.C. MacMillan, T.M. McIntire, J.A. Freites, D.J. Tobias, S.A. Nizkorodov, Interaction of water vapor with the surfaces of imidazolium-based ionic liquid nanoparticles and thin films, J. Phys. Chem. B 116 (2012) 11255–11265.
[18] B.F. Goodrich, J.C. de la Fuente, B.E. Gurkan, Z.K. Lopez, E.A. Price, Y. Huang, J.F. Brennecke, Effect of water and temperature on absorption of CO_2 by amine-functionalized anion-tethered ionic liquids, J. Phys. Chem. B 115 (2011) 9140–9150.
[19] M. Kanakubo, T. Umecky, T. Aizawa, Y. Kurata, Water-induced acceleration of transport properties in hydrophobic 1-butyl-3-methylimidazolium hexafluorophosphate ionic liquid, Chem. Lett. 34 (2005) 324–325.
[20] J.C. Araque, S.K. Yadav, M. Shadek, M. Maroncelli, C.J. Margulis, How is diffusion of neutral and charged tracers related to the structure and dynamics of a room-temperature ionic liquid? Large deviations from Stokes–Einstein behavior explained, J. Phys. Chem. B 119 (2015) 7015–7029.
[21] J.C. Araque, R.P. Daly, C.J. Margulis, A link between structure, diffusion and rotations of hydrogen bonding tracers in ionic liquids, J. Chem. Phys. 144 (2016), 204504.
[22] R.P. Daly, J.C. Araque, C.J. Margulis, Communication: stiff and soft nano-environments and the "octopus effect" are the crux of ionic liquid structural and dynamical heterogeneity, J. Chem. Phys. 147 (2017), 061102.
[23] A.L. Sturlaugson, K.S. Fruchey, M.D. Fayer, Orientational dynamics of room temperature ionic liquid/water mixtures: water-induced structure, J. Phys. Chem. B 116 (2012) 1777–1787.
[24] T. Köddermann, R. Ludwig, D. Paschek, On the validity of Stokes-Einstein and Stokes-Einstein-Debye relations in ionic liquids and ionic-liquid mixtures, ChemPhysChem 9 (2008) 1851–1858.
[25] I. Skarmoutsos, D. Dellis, R.P. Matthews, T. Welton, P.A. Hunt, Hydrogen bonding in 1-butyl-and 1-ethyl-3-methylimidazolium chloride ionic liquids, J. Phys. Chem. B 116 (2012) 4921–4933.
[26] I. Skarmoutsos, T. Welton, P.A. Hunt, The importance of timescale for hydrogen bonding in imidazolium chloride ionic liquids, Phys. Chem. Chem. Phys. 16 (2014) 3675–3685.
[27] P.A. Hunt, C.R. Ashworth, R.P. Matthews, Hydrogen bonding in ionic liquids, Chem. Soc. Rev. 44 (2015) 1257–1288.
[28] K. Fumino, A. Wulf, R. Ludwig, Hydrogen bonding in protic ionic liquids: reminiscent of water, Angew. Chem. Int. Ed. 48 (2009) 3184–3186.
[29] K. Fumino, T. Peppel, M. Geppert-Rubczynska, D.H. Zaitsau, J.K. Lehmann, S.P. Verevkin, M. Köckerling, R. Ludwig, The influence of hydrogen bonding on the physical properties of ionic liquids, Phys. Chem. Chem. Phys. 13 (2011) 14064–14075.
[30] K. Fumino, A. Wulf, R. Ludwig, The cation–anion interaction in ionic liquids probed by far-infrared spectroscopy, Angew. Chem. Int. Ed. 47 (2008) 8731–8734.
[31] S. Gehrke, M. von Domaros, R. Clarck, O. Hollóczki, M. Brehm, T. Welton, A. Luzar, B. Kirchner, Structure and lifetimes in ionic liquids and their mixtures, Faraday Discuss. 206 (2018) 219–245.
[32] L. Cammarata, S.G. Kazarian, P.A. Salter, T. Welton, Molecular states of in room temperature ionic liquids, Phys. Chem. Chem. Phys. 3 (2001) 5192–5200.
[33] A. Mele, C.D. Tran, S.H. De Paoli Lacerda, The structure of a room-temperature ionic liquid with and without trace amounts of water: the role of C-H…O and C-H…F interactions in 1-n-butyl-3-methylimidazolium tetrafluoroborate, Angew. Chem. Int. Ed. 42 (2003) 4364–4366.

[34] H.E. Bailey, Y.-L. Wang, M.D. Fayer, Impact of hydrogen bonding on the dynamics and structure of protic ionic liquid/water binary mixtures, J. Phys. Chem. B 121 (2017) 8564–8576.
[35] S. Agrawal, H.K. Kashyap, Structures of binary mixtures of ionic liquid 1-butyl-3-methylimidazolium bis(trifluoromethylsulfonyl)imide with primary alcohols: the role of hydrogen-bonding, J. Mol. Liq. 261 (2018) 337–349.
[36] Q.R. Sheridan, W.F. Schneider, E.J. Maginn, Anion dependent dynamics and water solubility explained by hydrogen bonding interactions in mixtures of water and aprotic heterocyclic anion ionic liquids, J. Phys. Chem. B 120 (2016) 12679–12686.
[37] S.N. Johnson, C.R. Hutchison, C.M. Williams, C.L. Hussey, G.S. Tschumper, N.I. Hammer, Intermolecular Interactions and Vibrational Perturbations within Mixtures of 1-Ethyl-3-methylimidazolium Thiocyanate and Water, J. Phys. Chem. C. (2018)https://doi.org/10.1021/acs.jpcc.8b07114.
[38] M.S. Kelkar, E.J. Maginn, Effect of temperature and water content on the shear viscosity of the ionic liquid 1-ethyl-3-methylimidazolium bis (trifluoromethanesulfonyl)imide as studied by atomistic simulations, J. Phys. Chem. B 111 (2007) 4867–4876.
[39] Y. Huang, Z. Wan, Z. Yang, Y. Ji, L. Li, D. Yang, M. Zhu, X. Chen, Concentration-dependent hydrogen bond behavior of ethylammonium nitrate protic ionic liquid–water mixtures explored by molecular dynamics simulations, J. Chem. Eng. Data 62 (2017) 2340–2349.
[40] A.R. Porter, S.Y. Liem, P.L.A. Popelier, Room temperature ionic liquids containing low concentrations—a molecular dynamics study, Phys. Chem. Chem. Phys. 10 (2008) 4240–4248.
[41] P.L. Kramer, C.H. Giammarco, M.D. Fayer, Dynamics of water, methanol, and ethanol in a room temperature ionic liquid, J. Chem. Phys. 142 (2015), 212408.
[42] J.E. Thomaz, C.M. Lawler, M.D. Fayer, The influence of water on the alkyl region structure in variable chain length imidazolium-based ionic liquid/water mixtures, J. Phys. Chem. B 120 (2016) 10350–10357.
[43] C.H. Giammarco, P.L. Kramer, M.D. Fayer, Ionic liquid versus Li(+) aqueous solutions: water dynamics near bistriflimide anions, J. Phys. Chem. B 120 (2016) 9997–10009.
[44] W. Smith, T.R. Forester, DL_POLY_2.0: a general-purpose parallel molecular dynamics simulation package, J. Mol. Graph. 14 (1996) 136–141.
[45] L. Martínez, R. Andrade, E.G. Birgin, J.M. Martínez, PACKMOL: a package for building initial configurations for molecular dynamics simulations, J. Comput. Chem. 30 (2009) 2157–2164.
[46] M.P. Allen, D.J. Tildesley, Computer Simulations of Liquids, Oxford University Press, Oxford, 1987.
[47] W.G. Hoover, Canonical dynamics: equilibrium phase-space distributions, Phys. Rev. A 31 (1985) 1695.
[48] W.G. Hoover, Constant-pressure equations of motion, Phys. Rev. A 34 (1986) 2499–2500.
[49] N.-T. Van-Oanh, C. Houriez, B. Rousseau, Viscosity of the ionic liquid from equilibrium and nonequilibrium molecular dynamics, Phys. Chem. Chem. Phys. 12 (2010) 930–936.
[50] H.J.C. Berendsen, J.R. Grigera, T.P. Straatsma, The missing term in effective pair potentials, J. Phys. Chem. 91 (1987) 6269.
[51] C. Cadena, J.L. Anthony, J.K. Shah, T.I. Marrow, J.F. Brennecke, E.J. Maginn, Maginn, Why Is CO2 So Soluble in Imidazolium-Based Ionic Liquids? J. Am. Chem. Soc. 126 (2004) 5300–5308.
[52] J.N. Canongia Lopes, A.A.H. Padua, Molecular force field for ionic liquids composed of triflate or bistriflylimide anions, J. Phys. Chem. B 108 (2004) 16893–16898.
[53] W. Smith, T.R. Forester, Parallel macromolecular simulations and the replicated data strategy: II. The RD-SHAKE algorithm, Comput. Phys. Commun. 79 (1994) 63–77.
[54] J.P. Ryckaert, G. Ciccotti, H.J.C. Berendsen, Numerical integration of the cartesian equations of motion of a system with constraints: molecular dynamics of n-alkanes, J. Comp. Phys. 23 (1977) 327–341.
[55] I. Skarmoutsos, E. Guardia, Local structural effects and related dynamics in supercritical ethanol. 1. Mechanisms of local density reorganization and residence dynamics, J. Phys. Chem. B 113 (2009) 8887–8897.
[56] A. Luzar, D. Chandler, Hydrogen-bond kinetics in liquid water, Nature 379 (1996) 55–57.
[57] V.H. Paschoal, L.F.O. Faria, M.C.C. Ribeiro, Vibrational spectroscopy of ionic liquids, Chem. Rev. 117 (2017) 7053–7112.
[58] E. Guardia, I. Skarmoutsos, M. Masia, Hydrogen bonding and related properties in liquid water: a Car–Parrinello molecular dynamics simulation study, J. Phys. Chem. B 119 (2015) 8926–8938.
[59] M. Holz, S.R. Heil, A. Sacco, Temperature-dependent self-diffusion coefficients of and six selected molecular liquids for calibration in accurate ^{1}H NMR measurements, Phys. Chem. Chem. Phys. 2 (2000) 4740–4742.
[60] H. Tokuda, S. Tsuzuki, Md.A.B.H. Susan, K. Hayamizu, M. Watanabe, How ionic are room-temperature ionic liquids? An indicator of the physicochemical properties, J. Phys. Chem. B 110 (2006) 19593–19600.
[61] N. Yaghini, L. Nordstierna, A. Martinelli, Effect of water on the transport properties of protic and aprotic imidazolium ionic liquids – an analysis of self-diffusivity, conductivity, and proton exchange mechanism, Phys. Chem. Chem. Phys. 16 (2014) 9266–9275.
[62] P. Sippel, S. Krohns, D. Reuter, P. Lunkenheimer, A. Loidl, Importance of reorientational dynamics for the charge transport in ionic liquids, Phys. Rev. E 98 (2018), 052605.
[63] K. Geirhos, P. Lunkenheimer, M. Michl, D. Reuter, A. Loidl, Communication: conductivity enhancement in plastic-crystalline solid-state electrolytes, J. Chem. Phys. 143 (2015), 081101.
[64] P. Debye, Polar Molecules, Dover Publications, New York, 1929.
[65] B.J. Berne, R. Pecora, Dynamic Light Scattering: With Applications to Chemistry, Biology and Physics, John Wiley & Sons, New York, 1976.
[66] A. Wulf, R. Ludwig, P. Sasisanker, H. Weingärtner, Molecular reorientation in ionic liquids: a comparative dielectric and magnetic relaxation study, Chem. Phys. Lett. 439 (2007) 323–326.
[67] C.D. de Michele, D. Leporini, Viscous flow and jump dynamics in molecular supercooled liquids. II. Rotations, Phys. Rev. E 63 (2001), 036702.
[68] I. Skarmoutsos, M. Eddaoudi, G. Maurin, Peculiar molecular shape and size dependence of the dynamics of fluids confined in a small-pore metal-organic framework, J. Phys. Chem. Lett. 9 (2018) 3014–3020.
[69] M.G. Mazza, N. Giovambattista, F.W. Starr, H.E. Stanley, Relation between rotational and translational dynamic heterogeneities in water, Phys. Rev. Lett. 96 (2006), 057803.
[70] S.-H. Chong, W. Kob, Coupling and decoupling between translational and rotational dynamics in a supercooled molecular liquid, Phys. Rev. Lett. 102 (2009), 025702.
[71] C.A. Rumble, C. Uitvlugt, B. Conway, M. Maroncelli, Solute rotation in ionic liquids: size, shape, and electrostatic effects, J. Phys. Chem. B 121 (2017) 5094–5109.
[72] G. Lipari, A. Szabo, Effect of librational motion on fluorescence depolarization and nuclear magnetic resonance relaxation in macromolecules and membranes, Biophys. J. 30 (1980) 489–506.
[73] H.J. Bakker, J.L. Skinner, Vibrational spectroscopy as a probe of structure and dynamics in liquid water, Chem. Rev. 110 (2010) 1498–1517.
[74] D. Laage, J.T. Hynes, Do more strongly hydrogen-bonded water molecules reorient more slowly? Chem. Phys. Lett. 433 (2006) 80–85.
[75] D. Laage, J.T. Hynes, A molecular jump mechanism of water reorientation, Science 311 (2006) 832–835.
[76] T.E. Raptis, V.E. Raptis, J. Samios, New effective method for quantitative analysis of diffusion jumps, applied in molecular dynamics simulations of small molecules dispersed in short chain systems, J. Phys. Chem. B 111 (2007) 13683–13693.
[77] T.E. Raptis, V.E. Raptis, J. Samios, Quantitative study of diffusion jumps in atomistic simulations of model gas–polymer systems, Mol. Phys. 110 (2012) 1171–1178.